Supporting Information

Baudoin et al. 10.1073/pnas.1211706110

SI Materials and Methods

The experiments were performed in microchannels made using standard soft lithography techniques. First, a mold was etched by depositing a dry-film photoresist on a glass slide and exposing it to a UV lamp through a photomask. The film then was developed in an aqueous solution of potassium to yield the negative of the channel design. This then constituted a mold over which poly-dimethylsiloxane was poured and allowed to polymerize. This microchannel was then cut out and bonded on another glass slide by passing the two surfaces in an oxygen plasma.

We used perfluorodecalin (PFD) to form the liquid plugs because of its good wetting properties (contact angle ~23°) and inertness. PFD is a fluorocarbon oil with viscosity $\mu = 5.1 \times 10^{-3}$ Pa·s and surface tension $\gamma = 19.3 \times 10^{-3}$ N/m. The plugs were separated by air bubbles. The fluids were controlled using either a water column, whose height determined the pressure head, or a programmable pressure controller (Fluigent MFCS-8C, generously lent by Fluigent S.A.), which provided precise and programmable pressure control.

The microchannel geometry presented a narrow Y-shaped junction (width = 200 μm) upstream of the test section (Fig. 5). This narrow region provided the ability to form liquid plugs reliably. The channel width then increased downstream of this junction, thus reducing the plug length equivalently. This geometry therefore provided better control of plug formation and length than using channels with constant width.

Experiments were recorded with a high-speed camera (Photron Fastcam 1024 PCI) through a stereomicroscope at 0.7× magnification. The resolution of the camera was $1,024 \times 1,024$ pixels, which yielded 1 pixel for 24.8 μm. The camera allowed image sequences to be captured at frame rates up to 1,000 images per second at full resolution. Image analysis was then performed using ImageJ software.

SI Model of Plug Motion and Rupture

In this section, we develop an analytical model to describe the motion of the gas–liquid train as the plugs change in size and eventually rupture in a straight channel. In this model, we ignore the effects of gravity and inertia by recalling that the Bond and Weber numbers are small. Moreover, because the experiments take place at small to moderate Reynolds and capillary numbers (Table S2), we limit ourselves to a minimal one-dimensional model that treats the plugs as discrete resistors. The aim, therefore, is not to describe the hydrodynamic behavior of our system in detail but to capture the essential mechanisms that lead to the cascade of ruptures.

As in the main text, we suppose that the total resistance to flow can be written as the sum of the resistances for individual plugs, which in turn can be separated into three contributions (1). The first one, R^v, is due to viscous dissipation in the bulk of the liquid; the other two correspond to capillary resistance at the front and rear interfaces, R^f and R^r, respectively. We also note that the fluid velocity V is nearly conserved at all locations in the channel. We therefore write the balance between driving pressure and resistance to flow as:

$$\Delta P = \sum_k R_k V = \sum_k \left[R_k^v + R_k^f + R_k^r \right] V. \qquad \textbf{[S1]}$$

The theoretical description aims at estimating the different resistance terms and their coupling with the plug velocities. An event-driven model of the coupling yields the evolution in time of the velocities and resistances, as discussed in the main text.

Problem Formulation. We consider a train of N liquid plugs pushed at a constant pressure head ΔP in a straight rectangular microchannel of height h and width w. The variables, defined in Fig. S3, are the positions $x_k(t)$ of the plugs' rear interfaces (numbered from right to left, beginning with the most advanced one); their lengths $L_k(t)$; the radii $\varepsilon_k^r(t)$ and $\varepsilon_k^f(t)$ of their rear and front menisci; and the cross-sectional area $S(x,t)$ of the lumens open to air at position x between the plugs. This description of the meniscus shape introduces two effects in the one-dimensional model developed here. First, the radii ε^f and ε^r determine the location at which fluid is exchanged with the films on the walls. Second, the front–rear asymmetry between the two curvatures leads to an additional resistance to flow, as described below.

The plugs leave a liquid film on the walls, whose thickness is variable: we define the cross-sectional area open to air behind plug k as $S_k^r(t) = S(x_k - \varepsilon_k^r, t)$, whereas one has $S_k^f = S(x_k + L_k + \varepsilon_k^f, t)$ in front of the plug. The amount of liquid deposited on the wall behind each plug depends on its velocity V_k (2–4), defined as the speed of its rear interface, $V_k(t) = dx_k(t)/dt$. On the other hand, the plug velocities are related to the flow rate $Q(t)$ through $V_k(t) = Q(t)/S_k^r(t)$.

The velocity of each plug may be different from its neighbors in principle, because they each can leave a film of different thickness. Nevertheless, experimental observations show that the plug velocities remain within less than 10% of one another for all experiments, as shown, for example, in Fig. S4 or observed in Figs. 2 and 3 in the main text. In the present model, the problem therefore is simplified by assuming that the plugs all travel at the same velocity $V(t)$, which comes to equating the thickness of the rear films. Therefore, we can simplify the notation by writing $S_k^r(V_k) = S^r(V)$.

Based on the parameters above, the dimensionless equations are obtained by introducing a characteristic length $\ell = \sqrt{wh}$, a characteristic pressure $\Delta P = 2\sigma/\ell$, and the viscocapillary timescale $\tau = \mu\ell/\sigma$. Using these definitions, the dimensionless speed of the plug train is just the capillary number $Ca = \mu V/\sigma$. In the following text, variables with tildes indicate dimensionless quantities.

Evolution of plug lengths. The equation giving the variation of the plug length as a function of time is obtained by expressing a balance between the fluid collected from the previous plug and the fluid left behind. Let $S_0 = wh = \ell^2$, then, during a time interval δt the length of the plug changes by δL, the volume of the plug changes by $S_0 \delta L$, the fluid collected ahead is $(S_0 - S_k^f)V\delta t$, and the fluid left behind is $(S_0 - S^r(V))V\delta t$; hence,

$$S_0 \delta L = \left(S_0 - S_k^f \right)V\delta t - (S_0 - S^r(V))V\delta t. \qquad \textbf{[S2]}$$

After simplification, rewriting Eq. **S2** in dimensionless form yields

$$\frac{d\tilde{L}_k}{d\tilde{t}} = \left[\tilde{S}^r(Ca) - \tilde{S}_k^f\left(\tilde{X}, \tilde{t}\right) \right] Ca. \qquad \textbf{[S3]}$$

A relation between $\tilde{S}^r$ and the capillary number Ca can be obtained by combining the scaling law proposed by Aussillous and Quéré (5) for the thickness of the liquid layer left behind a moving plug in a cylindrical channel and the empirical extension of this formula obtained by de Lózar et al. (6) for rectangular channels. By noting that $1 - \tilde{S}^r$ is nothing but what they call the wet fraction, we obtain

$$\tilde{S}^r = 1 - \frac{A + B\,\widehat{Ca}^{2/3}}{1 + C\,\widehat{Ca}^{2/3}}, \qquad \textbf{[S4]}$$

where A, B, and C are constants and

$$\widehat{Ca} = \left[1 + 0.12(\alpha - 1) + 0.018(\alpha - 1)^2\right] Ca$$

is an effective capillary number correcting for the departure of the aspect ratio $\alpha = w/h$ away from the square case $\alpha = 1$. The best fit with the experimental data displayed in figure 3 in ref. 6 for $\alpha = 12$ provides $A = 0.021$, $B = 3.4$, and $C = 5.2$ in the range of capillary numbers of interest.

The section of air in front of each plug $\tilde{S}_k^f$ is obtained by keeping track of the amount of liquid left on the wall by the preceding plug.

Pressure balance and plug velocities. A second set of equations is obtained by equilibrating the driving pressure head with the pressure drops from viscous dissipation in the bulk of the liquid plugs $\Delta\tilde{P}_v$ and at the successive liquid–air interfaces $\Delta\tilde{P}_i$:

$$\Delta\tilde{P} = \Delta\tilde{P}_v + \Delta\tilde{P}_i. \qquad \textbf{[S5]}$$

The viscous pressure drop is obtained by recalling the pressure-flow rate relation for a single fluid flowing in a rectangular channel (7):

$$\Delta P_v = \frac{12\mu}{wh^3} QL, \qquad \textbf{[S6]}$$

where Q is the flow rate and L is the length of the plug. It is common to extend this formula to account for the viscous pressure drop in a train of plugs, when they are sufficiently long and sufficiently far apart, by summing the individual contributions (see, e.g., ref 1):

$$\Delta P_v = \sum_k \frac{12\mu}{wh^3} QL_k. \qquad \textbf{[S7]}$$

Recalling that $Q = S^r V$, in dimensionless form Eq. **S7** reads:

$$\Delta\tilde{P}_v = 6\,Ca\,\tilde{S}^r \alpha \sum_k \tilde{L}_k. \qquad \textbf{[S8]}$$

The interface pressure differences are the result of deformations of the interfaces away from their static shapes. Indeed, for plugs at rest, curvatures at the front and the rear compensate their effects, leading to a uniform pressure within each plug. When the plugs move, interfaces depart from their static shapes, which leads to pressure drop corrections at both the front and rear interfaces, $\Delta\tilde{P}_i^f$ and $\Delta\tilde{P}_i^r$, respectively:

$$\Delta\tilde{P}_i = \Delta\tilde{P}_i^f + \Delta\tilde{P}_i^r. \qquad \textbf{[S9]}$$

Quantity $\Delta\tilde{P}_i^r$ can be estimated from the study of an air finger flowing in a channel, viewed as the tip of the following air bubble. The formula obtained by Bretherton (2), valid at low capillary numbers for a cylindrical tube, has been extended by Wong et al. (3) for a square channel, and more recently to the rectangular case by Hazel and Heil (4). By means of numerical simulations, these authors have shown that $\Delta P^r(\alpha, Ca) = f(\alpha)\Delta P^r(\alpha = 1, Ca)$, tabulating $f(\alpha)$ for $\alpha \in [1, 2]$. It turns out that in this range, their data are well fitted by the expression $\alpha f(\alpha) = 1 + 0.52(\alpha - 1)$, that is, $f(\alpha) = 0.52 + 0.48/\alpha$. This expression is not surprising because the pressure difference

should scale as the shear with, in a first approximation, additive contributions from the two directions, cross-stream in $1/h$ and spanwise in $1/w = 1/\alpha h$. Accordingly, we are confident that the extrapolation to our conditions $\alpha = 12.7$ is reliable.

On the other hand, Hazel and Heil have corrected the result of Wong et al. (3) for the finiteness of Ca. Their data for the dynamical contribution to ΔP in a square channel are in the form $DCa^{2/3}$, where D is a constant. Our fitting of their data in figure 8 of ref. 4, over the range $Ca \in [10^{-3}, 0.3]$, yields $D = 4.1$. Turning to dimensionless quantities, we finally obtain

$$\Delta\tilde{P}_i^r = D\alpha^{1/2}f(\alpha)Ca^{2/3}$$

[and $D\alpha^{1/2}f(\alpha) = 8.1$ for $\alpha = 12.7$]. Thus, for a set of N plugs moving at the same velocity, we obtain:

$$\Delta\tilde{P}_i^r = ND\alpha^{1/2}f(\alpha)Ca^{2/3}. \qquad \textbf{[S10]}$$

Finally, as to the front interfaces, following Ody et al. (8) and assuming that the apparent dynamic contact angle θ^a of the front meniscus [as defined by Chebbi (9)] is the same in the two principal directions, the pressure jump at the front interface of a single plug can be computed from

$$\Delta P_i^f = \sigma\left[\frac{2}{w} + \frac{2}{h}\right](1 - \cos\theta^a). \qquad \textbf{[S11]}$$

The apparent contact angles of each plug are not necessarily identical because the macroscopic films covering the channel wall ahead of them may be different. The dimensionless expression for the train of plugs then reads

$$\Delta\tilde{P}_i^f = \sum_k \frac{h + w}{\ell}(1 - \cos\theta_k^a). \qquad \textbf{[S12]}$$

The first plug moves on a dry substrate, with an apparent dynamic contact angle obtained from the Hoffman-Tanner law (10, 11):

$$\theta_1^a = ECa^{1/3}, \qquad \textbf{[S13]}$$

in which the constant E has been determined for PFD plugs moving in rectangular microchannels by Ody et al. (8) as $E = 4.9$. The following plugs move on a substrate that is prewetted by a macroscopic film. According to Chebbi (9), the apparent dynamic contact angle at the front of a plug advancing in a cylindrical tube of radius R over a fluid film of thickness e_∞ far away from the meniscus is given by

$$\tan\theta^a = (3Ca)^{1/3}F\left((3Ca)^{-2/3}\tilde{e}\cos\theta^a\right), \qquad \textbf{[S14]}$$

where

$$F(y) = \sum_{j=0}^{3} b_n[\log_{10}y]^n, \qquad \textbf{[S15]}$$

where $\tilde{e} = e_\infty/R$ and the b_n are tabulated in ref. 9; values rounded to two significant figures are given here for the reader's convenience: $b_0 = 1.4$, $b_1 = -0.59$, $b_2 = -3.2 \times 10^{-2}$, and $b_3 = 3.1 \times 10^{-3}$. To adapt this formula to our case, we estimate the relative fluid thickness $\tilde{e}$ as $(1 - \tilde{S}_k^f)^{1/2}$. Furthermore, because apparently no extension of this formula to the rectangular geometry exists, we introduce an empirical correction coefficient K so that in dimensionless form, we obtain

$$\tan\theta_k^a = K(3\text{Ca})^{1/3}F\left((3\text{Ca})^{-2/3}\left(1-\tilde{S}_k^f(\tilde{X},\tilde{t})^{1/2}\right)\cos\theta_k^a\right). \quad \textbf{[S16]}$$

The coefficient K, the only quantity not directly extracted from the literature, has been fixed to adjust time scales in the simulations to those of the laboratory experiments. We find $K \simeq 1.3$.

Plug dynamics. The equations derived above allow us to solve the coupled problem of the plug lengths and liquid deposition, resistance to flow, and plug velocity. By inverting this system, one obtains the capillary number at each time and thus computes the positions of the plugs. The model therefore provides a closed set of equations used to predict the dynamics of a train of plugs pushed at constant pressure head.

Application. The formulation above now can be expanded to be solved numerically. Eqs. **S8** and **S10** allow us to write

$$R_v = \frac{2\mu}{\ell}\left[6\tilde{S}^r\ \alpha\sum_k \tilde{L}_k\right], \quad \textbf{[S17]}$$

$$R^r = \frac{2\mu}{\ell}ND\alpha^{1/2}f(\alpha)\text{Ca}^{-1/3}. \quad \textbf{[S18]}$$

At low capillary number, expanding Eqs. **S12** and **S16** at lowest order yields

$$\Delta\tilde{P}_i^f = \frac{h+w}{2\ell}\sum_k \theta_k^{a2}, \quad \textbf{[S19]}$$

$$\theta_k^a = K(3\text{Ca})^{1/3}F\left((3\text{Ca})^{-2/3}\left(1-\tilde{S}_k^f(\tilde{X},\tilde{t})^{1/2}\right)\right), \quad \textbf{[S20]}$$

which leads to

$$R^f = \frac{\mu}{\ell}\left[\frac{h+w}{\ell}\right]\text{Ca}^{-1/3}\left[12+3^{2/3}K^2\sum_{k=2}^N F^2\left((3\text{Ca})^{-2/3}\left(1-\tilde{S}_k^f(\tilde{X},\tilde{t})^{1/2}\right)\right)\right].$$
$$\textbf{[S21]}$$

Fig. S5 displays the predicted variation of the front interface resistance of a single plug moving in a prewetted channel as a function of the capillary number for different relative thicknesses of the macroscopic film ahead of the plug $\tilde{e}$. It shows that Eq. **S20**, which is the lowest-order approximation to Eq. **S16**, gives sufficiently accurate results in the range of capillary numbers of interest. Accordingly we may rely on Eq. **S21**, which both provides a better insight into the physics of the problem and is simpler to implement. The important phenomenon to be seen in Fig. S5 is the systematic decrease of the front interface resistance with $\tilde{e}$ for all values of the capillary number, which we call the "lubrication effect."

Finally, Fig. S6 shows the variation of the total interfacial resistance $R_i = R_i^f + R_i^r$ of the first plug (dashed curve) and the following plugs (full lines) as a function of the capillary number Ca and the relative thickness of the liquid film $\tilde{e}$. A monotonic decrease of the interfacial resistance is observed when the capillary number increases for all values of $\tilde{e}$ between 10^{-1} and 10^{-5}, as well as for the dry substrate ($\tilde{e}=0$).

Physical Origin of the Cascade. Initially, a train of plugs is created by alternately pushing some air and some liquid in a Y-junction with low input pressure. The initial state therefore is a set of N plugs separated by air bubbles coated by a thin layer of liquid, with dry substrate ahead of the first plug. When a large pressure head ΔP is applied at the beginning of an experiment, all the liquid plugs leave a larger amount of liquid on the walls than what they may recover from the liquid film ahead of them. The amount of liquid left indeed increases with the capillary number, according to Eq. **S4**. This leads to a decrease in the plugs' length, Eq. **S3**, and thus of the viscous resistance, Eq. **S17**. Because $\Delta P = RV$ and the pressure head is constant, this resistance decrease induces an increase in the plug velocity. In turn, this velocity increase is exacerbated by the decrease in the interface resistance $R_i = R_i^f + R_i^r$ (Fig. S6). Another phenomenon contributing to the reduction of the front interface resistance is the lubrication effect generated by the interplug liquid film. As its thickness increases with the plug velocity, a further reduction in the front interface resistance results (Fig. S5).

Finally, each plug rupture provokes a brutal decrease in the interfacial resistance due to the reduction in the number of interfaces, which locally thickens the prewetting film. This leads to a large acceleration of the plugs and thus to more and more plug ruptures.
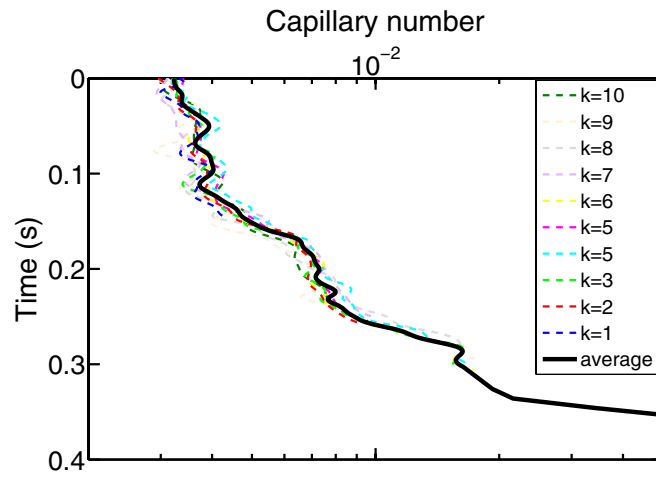
Computation. The system of equations has been solved using an event-driven code: Between two plug ruptures, the system is solved by a finite difference method. Each time a rupture takes place, the interfacial resistance is updated. Owing to the large increase in the plug velocities, mesh refinement was performed to determine the time step between two computations and to maintain accuracy.

Input Parameters. Table S1 summarizes the parameters used in our simulations. Using the value of the capillary number shown in Fig. S4 for the capillary number, which corresponds to a maximum velocity of $V \simeq 4\times 10^{-2}$ m/s, we obtain the estimates quoted in Table S2 for the dimensionless parameters of the problem.

1. Baroud CN, Gallaire F, Dangla R (2010) Dynamics of microfluidic droplets. *Lab Chip* 10 (16):2032–2045.
2. Bretherton FP (1971) The motion of long bubbles in tubes. *J Fluid Mech* 10(2):166–188.
3. Wong H, Radke CJ, Morris S (1995) The motion of long bubbles in polygonal capillaries. Part. 2. Drag, fluid pressure and fluid flow. *J Fluid Mech* 292:95–110.
4. Hazel AL, Heil M (2002) The steady propagation of a semi-infinite bubble into a tube of elliptical or rectangular cross-section. *J Fluid Mech* 470:91–114.
5. Aussillous P, Quéré D (2000) Quick deposition of a fluid on the wall of a tube. *Phys Fluids* 12(10):2367–2371.
6. de Lózar A, Hazel AL, Juel A (2007) Scaling properties of coating flows in rectangular channels. *Phys Rev Lett* 99(23):234501.
7. White FM (1991) *Viscous Fluid Flow* (McGraw-Hill, New York), 2nd Ed.
8. Ody CP, Baroud CN, de Langre E (2007) Transport of wetting liquid plugs in bifurcating microfluidic channels. *J Colloid Interface Sci* 308(1):231–238.
9. Chebbi R (2003) Deformation of advancing gas-liquid interfaces in capillary tubes. *J Colloid Interface Sci* 265(1):166–173.
10. Hoffman RL (1975) Study of advancing interface. A. Interface shape in liquid-gas systems. *J Colloid Interface Sci* 50(2):228–241.
11. Tanner LH (1979) Spreading of silicone oil drops on horizontal surfaces. *J. Phys. D* 12(9): 1473.

Fig. S1. Dynamics of a set of polydisperse plugs pushed at constant pressure head 4.8 kPa. (*A* and *B*) Plug positions as functions of time, experimental and simulated, respectively. The variation in the capillary number with time is given to the right of *A*, where the gray dashed line indicates the time when several plugs break almost simultaneously.

Fig. S2. Influence of bifurcations on the fluid redistribution in the network. (*A* and *B*) Two sequences show the evolution of plugs inside the last five generations of the network driven at a pressure head of 3.5 kPa with slightly different timing. In *A*, the liquid plug in the first generation divides before the cascade takes place; thus, only one of the daughter plugs is broken while the adjacent path is reinforced by the other daughter. In *B*, the plug ruptures before the bifurcation and the adjacent path remains weakened. The time separating the two images is 14 ms.

Fig. S3. Sketch of the problem, showing plug k surrounded by plugs $k-1$ and $k+1$. Liquid is shown in white and air in gray. The moving plugs (velocity $V_k = dx_k/dt$) leave a film behind them thicker than the film they encounter in front. The cross-sectional area open to air behind plug k (S_k^r) therefore may be different from the air surface in front (S_k^f). The wetting liquid forms menisci of radius ε^r at the rear and ε^f at the front.

Fig. S4. Evolution of the capillary number $\mu V_k/\sigma$ associated with the rear interface of 10 plugs pushed at a constant pressure head 4.8 kPa. Each dashed line corresponds to the capillary number of a given plug k, and the plain line corresponds to the capillary averaged over all the plugs. This figure corresponds to Fig. 3 in the main text.
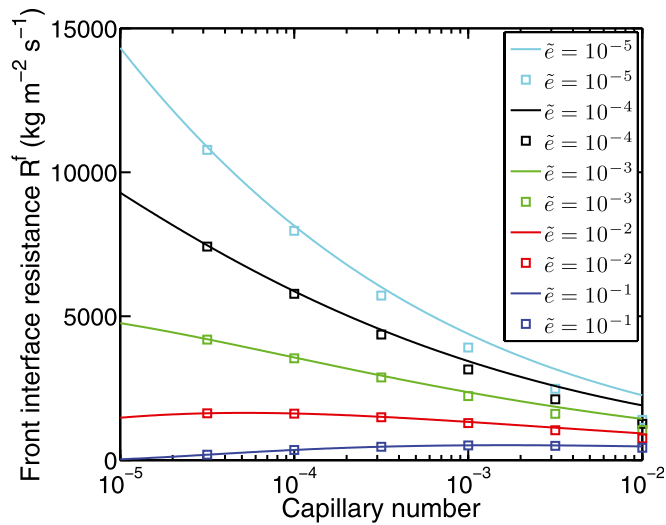

Fig. S5. Evolution of the front interface resistance of a plug moving in a prewetted channel as a function of the capillary number Ca for different values of the relative thickness of the macroscopic film preceding the plug $\bar{e}$. The squares correspond to solutions of the exact (Eq. **S16**) and the lines to its lowest-order expansion (Eq. **S20**).

Fig. S6. Interfacial resistance $R_i = R_i^f + R_i^r$ of a single plug as a function of the capillary number Ca, moving on a substrate either dry (dashed line) or prewetted by a macroscopic film for different relative thicknesses $\bar{e}$ (solid lines).

Table S1. Value of parameters used in our simulations

Parameter	Symbol	Value	Unit
Channel width	w	700	μm
Channel height	h	55	μm
Surface tension	σ	19.3×10^{-3}	N/m
Viscosity	μ	5.1×10^{-3}	kg/m·s^2
Density	ρ	2×10^3	kg/m^3

Table S2. Value of dimensionless parameters in the problem

Number	Formula	Maximum value
Re	$\rho V \ell / \mu$	10
Ca	$\mu V / \sigma$	10^{-2}
We	$\rho V^2 \ell / \sigma$	10^{-1}
Bo	$\rho g h^2 / \sigma$	0.2

Movie S1. Evolution of a single plug of initial length $L_0 = 740$ μm pushed at constant pressure head 2 kPa. Time is slowed by a factor of 250. This movie illustrates Fig. 1 in the main text.

Movie S1

Movie S2. Dynamics of a set of equally spaced monodisperse plugs. The initial length of the plugs is $L_{k,0} = 780$ μm, and the distance separating two adjacent plugs is $d_k \simeq 2$ mm. The whole train is pushed at constant pressure head 2.0 kPa. Time is slowed by a factor of 10. This movie illustrates Fig. 2 in the main text.

Movie S2

Movie S3. Dynamics of a set of polydisperse plugs pushed at constant pressure head 4.8 kPa. Time is slowed by a factor of 10. This movie illustrates Fig. 3 in the main text.

Movie S3
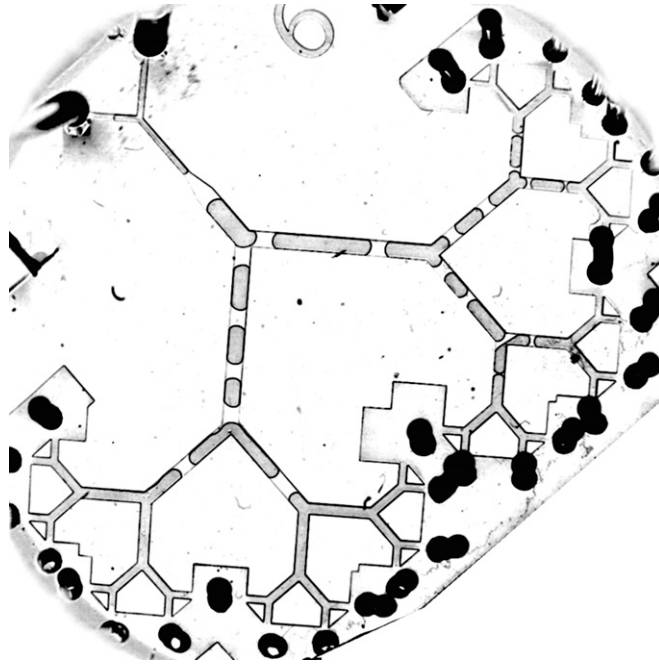
Movie S4. Dynamics of an initial set of liquid plugs pushed at a constant pressure head $\Delta P = 3.5$ kPa in a six-generation bifurcating network. Time is slowed by a factor of 10. This movie illustrates Fig. 5 in the main text.

Movie S4